Polymer Journal (2024) 56:915–924
https://doi.org/10.1038/s41428-024-00927-4

ORIGINAL ARTICLE

Carbon nanotubes functionalized with α-aminoisobutyric acid-containing peptide increase gene delivery efficiency in plant mitochondria

Simon Sau Yin Law[1] · Mako Kuzumoto[2] · Seiya Fujita[2] · Tsuyohiko Fujigaya[3] · Keiji Numata[1,2]

Received: 18 April 2024 / Revised: 21 May 2024 / Accepted: 21 May 2024 / Published online: 14 June 2024

Abstract

Functionalized carbon nanotubes have shown tremendous promise in the field of plant biotechnology for genetic engineering and cargo delivery; recent findings have shown that they can be delivered within specific organelles, such as mitochondria and chloroplasts, in intact plants. 2-Aminoisobutyric acid is an unnatural amino acid that promotes helical conformation and has been demonstrated to increase membrane permeability. Rational substitution of this amino acid into a mitochondrial targeting peptide induced a helical conformation that, when functionalized onto polymer-coated carbon nanotubes, conferred increased membrane permeability compared with that of the native peptide. The secondary structure was maintained on the surface and, when used to deliver pDNA, led to an increase in gene expression, suggesting that this method may be used to enhance the delivery efficiency of existing functional peptides.

Introduction

Genetic engineering of plants remains one of the most promising and economical approaches to scaling food and energy production for the world population and addressing limitations in food and energy production associated with climate change [1–3]. Biological applications using single-walled carbon nanotubes (SWNTs) have emerged as potential delivery tools for plants due to their wide biocompatibility and outstanding delivery efficiency [4–9]. SWNTs have been shown to be capable of crossing plant cell walls and membranes, likely due to their unique physical properties, including their high aspect ratio, surface area, and stiffness [7, 10]. In particular, SWNT-based nanocarriers have been shown to efficiently deliver nucleic acid cargo into intact plants without significant cytotoxicity [4, 8, 11–13].

In our previous work, we developed a polymer-coated SWNT (SWNT-PM) system conjugated with functional peptides for the delivery of intact pDNA into plant mitochondria [4]. We demonstrated that the application of a mitochondrial targeting peptide could be used for the specific delivery of pDNA into the mitochondria within intact plants for mitochondria-targeted gene expression [4, 14]. We also observed that the peptides conjugated to the SWNT-PM had a large effect on the delivery efficiency and subsequent gene expression of the system; in particular, the Cytcox peptide was required for both mitochondrial targeting and DNA delivery. Secondary structures are maintained on the surface of nanomaterials due to the physical properties observed in our previous studies; thus, we hypothesized that the modification of peptides conjugated on the surface of SWNT-PM nanocarriers (NCs) could be employed to achieve increased specificity and delivery efficiency [15, 16]. Our previous work also demonstrated that unnatural amino acids such as 2-aminoisobutyric acid (Aib) are able to efficiently cross cell membranes for cargo delivery through the interaction of the helical domains introduced [17–19].

Supplementary information The online version contains supplementary material available at https://doi.org/10.1038/s41428-024-00927-4.

✉ Keiji Numata
keiji.numata@riken.jp

[1] Biomacromolecules Research Team, RIKEN Center for Sustainable Resource Science, 2-1 Hirosawa, Wako, Saitama 351-0198, Japan

[2] Department of Material Chemistry, Graduate School of Engineering, Kyoto University, Kyoto Daigaku Katsura, Nishikyo-ku, Kyoto 615-8510, Japan

[3] Department of Applied Chemistry, Kyushu University, Nishi-ku, Fukuoka 819-0395, Japan

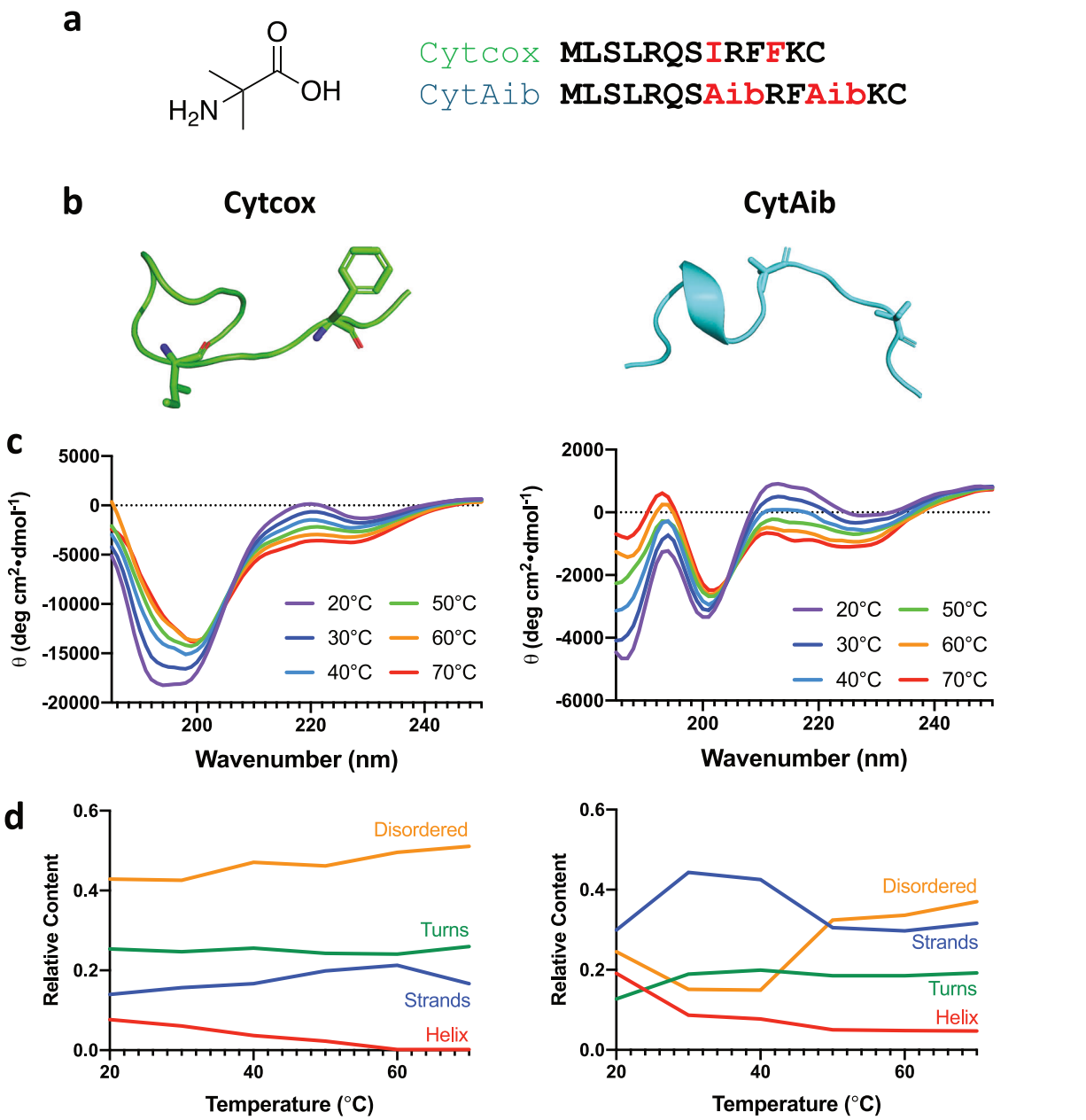

Fig. 1 Physical properties of Cytcox and CytAib. a Chemical structure of the nonnatural amino acid Aib and the amino acid sequence of the mitochondrial targeting peptide (Cytcox) with the Aib-substituted sequence (CytAib). **b** Secondary structures of the two peptides determined from PSIPRED structure prediction and AMBER- and GROMACS-based molecular dynamics simulations. **c** CD spectra of Cytcox and CytAib showing the respective spectra when heated from 20 to 70 °C at 10 °C intervals. **d** Overall secondary composition as the peptides are heated from 20 to 70 °C, as determined from the CD spectra in **c**

Aib is an unnatural nonproteinogenic amino acid that is rare in nature and is a strong helix inducer in peptides due to its Thorpe–Ingold effect as a result of its dimethyl group (Fig. 1a), and it has been previously demonstrated to induce helical structures in peptides as well as improve their ability to mediate the delivery of nucleic acids and other cargos into mammalian cells. We recently reported mitochondria-targeted gene delivery in plants such as *Arabidopsis thaliana* (*A. thaliana*) and *Nicotiana tabacum* (*N. tabacum*) as well as in human embryonic kidney (HEK) 293 cells using mitochondrial targeting signal (MTS)-fused peptides [4, 14, 19–21]. The first 12 residues of the presequence (Cytcox) in the yeast cytochrome c oxidase subunit IV were shown to facilitate translocation into the mitochondria, and the helical conformation of this peptide was found to be necessary for effective mitochondrial import, similar to most MTSs [19, 22, 23].

Aib residues in peptides often introduce kinks and helical secondary structures that can increase membrane permeability; thus, for this research, we investigated whether it would be possible to increase the membrane permeability of functionalized SWNT-PM by conjugating it with Aib-containing peptides. Aib-containing peptides are thought to mediate interactions between helical secondary structures through the disruption of cellular membranes through interactions between the introduced kinks and the membrane, increasing membrane permeability [17, 19]. The secondary structure characteristics were maintained even after conjugation to the SWNTs, and we also demonstrated that the Aib-containing peptides had significantly greater membrane permeability, as quantified by gene expression and intracellular localization assays using bright yellow tobacco (BY-2) cells. These results, along with intracellular and molecular dynamics simulations, suggest that increased permeability translates to increased gene expression, as determined by luciferase and GFP expression quantified by enzymatic activity and confocal microscopy, respectively. Based on these results, we predict that it would be possible to further increase the permeability of the previously developed nanomaterials by introducing cell-penetrating motifs to the conjugated peptides to increase their expression efficiency.

Experimental

Materials

Mitochondria-targeting (Cytcox) and DNA-binding (KH9) peptides (0.25 mM for Cytcox and 0.1 mM for KH9 conjugated to SWNTs) were synthesized by the Research Resources Center of RIKEN Brain Science Institute. Both peptides contained an additional Cys at the C-terminus for polymer conjugation. CytAib was synthesized via liquid-phase peptide synthesis and subsequently purified by high-performance liquid chromatography (HPLC) [24, 25]. The purity of the respective peptides was determined to be greater than 95%, as determined by HPLC (Supplementary Fig. S2).

Statistical analysis

GraphPad Prism 8.0 (GraphPad, USA) was used for statistical analysis and significance testing. The statistical tests used to compare the samples are outlined in their corresponding figure legends. Differences between two means were considered statistically significant at $P < 0.05$ and are indicated with asterisks (*) in the plots. Other P values and * notations used within the graphs are defined within the respective figures, and the exact P values for significance testing are listed within the respective figures. The experimental data are expressed as the mean ± standard deviation unless otherwise noted, and the sample sizes are listed in each respective figure.

Synthesis of SWNT-PM and SWNT-PM-Peptide

SWNT-PM was synthesized as previously described and outlined as follows [4, 26, 27]. Maleimide (0.855 g, 8.8 mmol; Tokyo Chemical Industry Co., Ltd., Japan) and furan (1.1 mL, 15 mmol; Tokyo Chemical Industry Co., Ltd., Japan) were stirred in water (10 mL) for 5 days and collected by vacuum filtration to yield crude furan-protected maleimide (FpM). Crude FpM (200 mg, 1.25 mmol) was dissolved in anhydrous THF (5 mL; Wako Pure Chemical Industries, Ltd., Japan), triphenylphosphine (375 mg, 1.43 mmol; Tokyo Chemical Industry Co., Ltd., Japan), and PEGMA (300 µL; Sigma–Aldrich, Japan). The mixture was transferred to an ice bath, and diethyl azodicarboxylate (0.65 mL, 1.43 mmol; Sigma–Aldrich, USA) was added dropwise to the reaction mixture and incubated for 24 h.

The solvent was then removed by vacuum evaporation, and the solution was redissolved in diethyl ether and extracted twice with water. The aqueous phases were collected and extracted with chloroform three times. Excess water was removed with the addition of excess $MgSO_4$ (Tokyo Chemical Industry Co., Ltd., Japan), and finally, the mixture of organic phases was purified by silica gel flash column chromatography to yield purified FpM.

SWNTs (5 mg; Carbon Nanotechnologies, Inc., USA) were dispersed in 0.2% w/w SDS solution (50 mL) using ultrasonication for 1 h and centrifuged at 60,000 × *g* for 1 h using an ultracentrifuge (Hitachi Himac). Approximately 2–3 mL of the supernatant was removed from the precipitated SWNTs, and the furan-protected maleimide purified earlier was added to the solution along with *N,N*-methylene bis(acrylamide) (10 mg; Tokyo Chemical Industry Co., Ltd., Japan). PEGMA solution (550 µL; Sigma–Aldrich, Japan) diluted with dH_2O was added to the supernatant (5 mL), and the mixture was stirred and bubbled with N_2 gas for 15 min. Tetramethylethylenediamine (TMEDA) (4.4 µL; Tokyo Chemical Industry Co., Ltd., Japan) and ammonium peroxodisulfate (20% w/w in dH_2O; Sigma–Aldrich, USA) were added dropwise through a needle under a N_2 atmosphere. The solution was allowed to react and was further stirred for 24 h.

The solution was then dialyzed using 10 kDa snakeskin dialysis tubing (Thermo Fisher, USA) for 3 days. Deprotection of the maleimide groups for thiol functionalization was achieved by heating at 75 °C for 2 h, and peptides (Cytcox 250 µM, CytAib 250 µM, and KH9 100 µM) were added to the deprotected SWNTs for functionalization at 16 °C for 24 h. Unreacted peptides and polymer-related

molecules were dialyzed using a 10 kDa Slide-a-Lyzer (Merck Millipore, USA) for 24 h to yield the respective SWNT-PM-Peptide and were stored at 4 °C prior to infiltration within *A. thaliana*.

Characterization of SWNT-PM NC and peptide samples

Circular dichroism spectroscopy measurements were performed using a JASCO J-820 spectropolarimeter and recorded from 250 to 185 nm (1 nm resolution) in a 1-mm path length quartz cuvette at a scan rate of 100 nm/min. Peptide-only samples were measured in dH_2O at 100 µM, and SWNT samples were measured directly in solution at 25 °C. Peptide stability was measured by heating the peptides from 20 °C to 70 °C at a rate of 2 °C/min, and measurements were taken at 10 °C intervals. The spectra were plotted using average values from 10 measurements, and the background was subtracted.

Atomic force microscopy (AFM) was performed on the respective SWNT samples on a graphite substrate using a Hitachi AFM 5300E (Hitachi High-Tech Science Cooperation, Japan). The samples were spotted on a graphite substrate (5 µL) and allowed to evaporate at room temperature for 1 h before being rinsed with Milli-Q water. The washed samples were then air-dried for 1 h before the AFM measurements. AFM observation was performed in air at 25 °C using a silicon cantilever (SI-DF3, Hitachi High-Tech Science Corporation, Japan) with a spring constant of 1.7 N m^{-1} in tapping mode. AFM height profiles were analyzed and quantified by Gwyddion (version 2.58) to quantitatively compare the differences in height after polymer and peptide functionalization.

Raman microscopy analyses of SWNT samples and SWNT-NC-infiltrated BY-2 cells were performed using a JASCO NRS-4500 Raman microscope (JASCO, Japan). Nanoparticle characterization was performed using SWNT-PM and SWNT-PM-Peptide aqueous samples at 100× magnification on a cover glass with a green laser at 532 nm and an integration time of 6 s per spectrum, with images collected over an area of 50 × 50 µm at 2 µm intervals. SWNT uptake was quantified by the normalized peak ratio between the G band at 2630 cm^{-1} and the alkyl region among all the infiltrated samples.

DNA binding of the SWNT NCs and the individual peptides (Cytcox, CytAib, and KH9) was determined by gel shift electrophoresis using pDNA (*pDONR-35S-GFP*). Twenty microliters of SWNT or peptide (250 or 25 µM) solution was incubated with 50 ng of pDNA for 30 min. The samples were subsequently mixed with 1× loading buffer before analysis on a 1% agarose gel in TAE buffer. The gel was then stained with ethidium bromide for 20 min before imaging at 254 nm. Quantification of the plasmid bands was performed using ImageJ Fiji (version 1.54; NIH).

For confirmation of peptide conjugation, the SWNT-PM-Peptides were subjected to alkaline hydrolysis (0.1 M NaOH) at 90 °C for 1 h to release the conjugated peptides. The reaction mixture was neutralized with one equivalent of HCl, and a total sample volume of 100 µL was injected for analysis via reversed-phase HPLC. The HPLC instrument was equipped with an autosampler (AS-2055, JASCO, Tokyo, Japan), gradient pump (PU2089, JASCO), column oven (CO-4060, JASCO), and C18 column (YMC-Triart C18, particle size 5 µm, 150 × 4.6 mm i.d., YMC, Kyoto, Japan).

The samples were eluted using a gradient of Milli-Q water (eluent A), acetonitrile (eluent B), and 1% (v/v) trifluoroacetic acid (TFA) (eluent C). The composition of the gradient was varied linearly from 85% eluent A, 5% eluent B, and 10% eluent C to 55% eluent A, 35% eluent B, and 10% eluent C over a period of 30 min at a flow rate of 1 mL/min and a column temperature of 25 °C. The elution of each sample was measured by the UV absorbance values at 220 and 260 nm and analyzed using chromatography software (ChromNAV, JASCO, Tokyo, Japan). The fractions corresponding to the peptide–polymer conjugates were collected and lyophilized for 48 h prior to MALDI analysis.

A MALDI–TOF spectrometer (Autoflex speed LRF; Bruker Daltonics, Billerica, MA, USA) operating in positive ion reflection mode at a 15 kV accelerating voltage was used to record the MALDI mass spectra of the polymer–peptide conjugates. The samples were prepared by mixing the lyophilized cleaved polymer–peptide conjugate samples with α-cyani-4-hydroxycin-namic acid (10 mg/mL) and trifluoroacetic acid (TFA) (0.1%) in a 1:1 ratio (5 µL total). The samples (2 µL) were transferred to MALDI MTP 384 ground steel BC target plates and dried at room temperature for 1 h before measurement.

MD simulations of the peptide and membrane interactions

Peptide structures containing unnatural amino acids were determined using AMBER-based molecular dynamics structure simulation for unnatural amino acids (PEPstrMOD) [28]. The secondary structures and β-turns were determined by PSIPRED and BetaTurns, respectively. Forcefield libraries (FFNCAA, FFPTM and SwissSideChain) were used to generate force fields for both canonical and unnatural amino acids, and the initial structure was generated using AMBER (version 11.0). The initial structure was subjected to energy minimization and molecular dynamics using GROMACS (version 4.6.5) to generate the final peptide structure. Cell membrane interactions were determined using CellPM with

energy-minimized structures. The transfer energy (ΔG(z)) was determined using a water and implicit solvent DOPC bilayer system [29].

Delivery of SWNT-PM-Peptide/pDNA complexes into A. thaliana

Seeds of *A. thaliana* Col-0 were stratified and germinated on 0.5 × Murashige and Skoog (MS) (Sigma–Aldrich; USA) medium plates under 16-/8-h light/dark periods at 22 °C. Seven-day-old *A. thaliana* plants were used to assess pDNA delivery and gene expression. SWNT-PM-Peptide/pDNA complexes were prepared by mixing 10 µg (3 mg/mL) of SWNT-PM-Peptide solution and 10 ng of pDNA at 25 °C for 30 min per seedling.

Vacuum/pressure infiltration was performed by incubating whole *A. thaliana* seedlings in the respective solutions, which were then subjected to 0.08 MPa vacuum and 0.08 MPa pressure for 60 s each. The seedlings were allowed to recover in the solution for 1 h at room temperature before being placed on their original 0.5 × ½ MS plates. The uptake of SWNT-PM-Peptide and the gene expression levels of the GFP and luciferase reporter constructs were assessed after overnight incubation (18 h).

The gene expression of the *RLuc* reporter construct was measured using a *Renilla* luciferase assay kit (Promega, Madison, WI) according to the manufacturer's protocol. Infiltrated seedlings that were incubated overnight were homogenized with 1 × Luciferase Assay Lysis Buffer (Promega). The lysate was centrifuged for 3 min at 13,000 × *g*, and 50 µL of the supernatant was mixed with *Renilla* Luciferase Assay Substrate and *Renilla* Luciferase Assay Buffer (Promega) at a 1:1 (v/v) ratio at the manufacturer's recommended concentrations. Luciferase activity was measured by photoluminescence (relative light units) using a luminometer (GloMax 20/20, Promega) with a standard accumulation time of 1 s. The amount of protein in the supernatant was determined via Bradford protein assays (Pierce Biotechnology, Rockford, IL) and was used to normalize the relative light units across the samples (RLU/mg) for expression comparisons. Background corrections were performed using the average RLU/mg value of untransfected seedlings and dH_2O samples.

Results and discussion

Physical characterization of Cytcox and CytAib

We first developed the Aib-containing Cytcox peptide through the substitution of two amino acids at positions 8 and 11 (Fig. 1a, b). The residues for substitution were selected based on their hydrophobicity to increase their intracellular solubility to improve functionalization [30, 31]. Furthermore, the substitution of Aib within peptides has been previously demonstrated to promote and stabilize helical structures due to the additional dimethyl group integrated as part of the peptide backbone; our previous research has also demonstrated that such substitutions have also worked efficiently at improving the translocation of substituted peptides through the translocase of the outer membrane (TOM) complex in plant cells [19]. Therefore, the introduction of Aib was expected to perturb the overall structure of the peptide by introducing helicity, which will likely improve its cell-penetrating ability. MD simulations of the respective peptides (Cytcox and CytAib) revealed that the introduction of Aib at positions 8 and 11 introduced beta-coil secondary structures within the peptides (Fig. 1b). These conformations reached relatively stable RMSDs, suggesting that minimal RMSDs had been reached (Supplementary Fig. S1).

This phenomenon was further investigated experimentally using circular dichroism (CD) measurements to further probe secondary structure changes induced by the introduction of Aib. We first measured the liquid-state CD spectra of the two peptides in solution to determine their overall secondary structure contents (Fig. 1c). Due to the stability afforded by the helix formation as a result of the Aib substitution, we also investigated the thermal stability of the respective peptides after heating them from 20 °C to 70 °C (Fig. 1c, d). As expected, based on the CD spectra, we observed a loss of secondary structure as a result of the increase in temperature, which is typically observed following peptide denaturation (Fig. 1d). Overall, the turn contents were similar between the two peptides, but the strand content markedly increased in CytAib at all the observed temperatures. We also observed that the introduction of Aib into the sequence significantly increased the helical structure from 8% to 20%, as measured by CD at 20 °C, matching well with the MD-simulated structures (Fig. 1b, d). This helical structure was lost upon heating for both peptides, and both peptides were mostly disordered at temperatures above 50 °C (Fig. 1c). We also observed a general decrease in thermal stability for the CytAib peptide relative to the Cytcox peptide, suggesting that the induced helical structures were likely to be less stable than the native helical structures, as reported in other studies [32, 33].

Conjugation of Aib-containing Cytcox to SWNT-PM

We then evaluated whether the physical properties of CytAib changed significantly upon SWNT conjugation in terms of DNA binding and physical characteristics. The conjugation of the respective peptides was performed as described in our previous studies, where the maleimide groups on the polymer surface were deprotected at 75 °C, followed by Michael addition to the thiol group on the respective C-terminal Cys

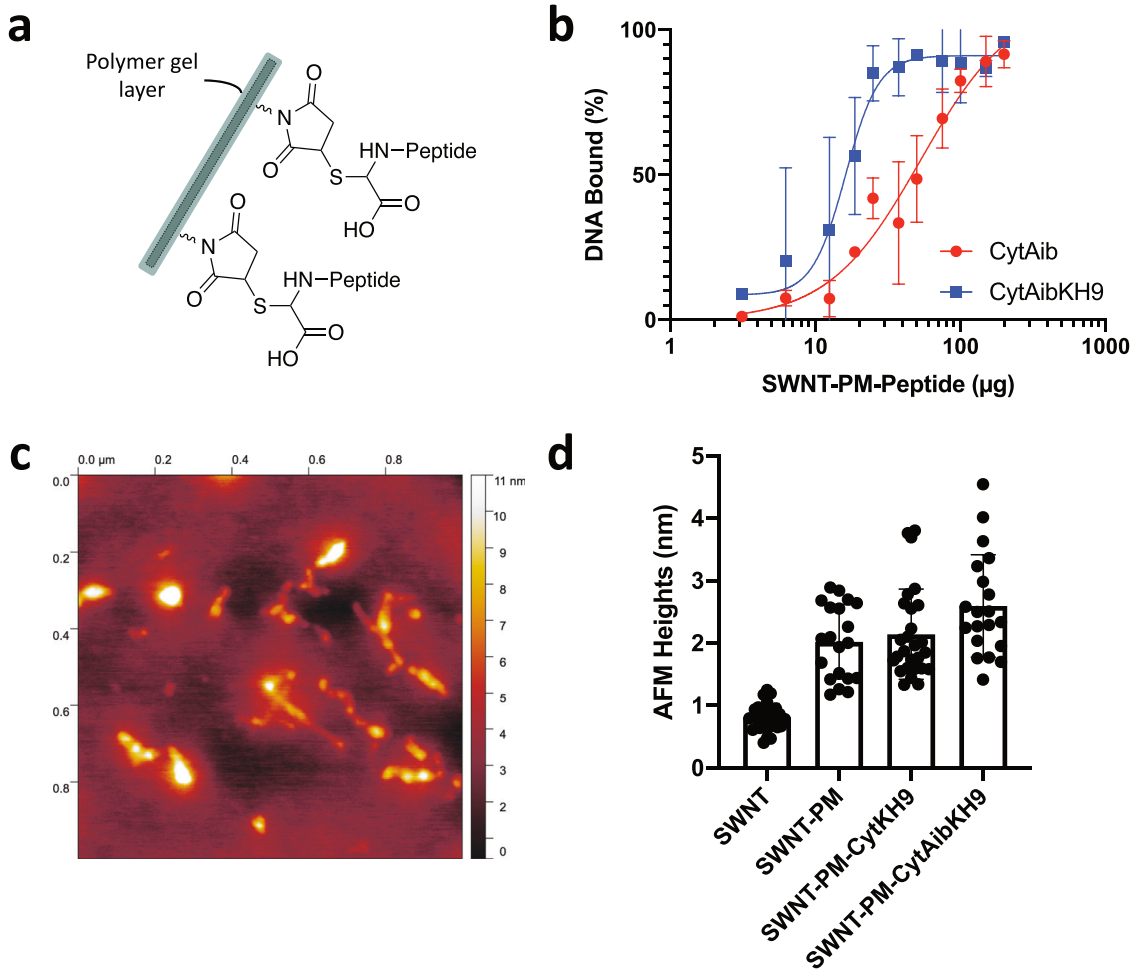

Fig. 2 Properties of CytAib conjugated to SWNT-PM. a Diagram of SWNT-PM-Peptide showing the thiol conjugation of each peptide to the maleimide groups on the SWNT surface. **b** DNA-binding abilities of SWNT-PM-CytAib and SWNT-PM-CytAibKH9. **c** Representative AFM image of SWNT-PM-CytAibKH9 cast on a graphite substrate. **d** Quantification of the AFM profiles of SWNT, SWNT-PM and SWNT-PM-Peptide NCs recorded on a graphite substrate ($n = 20$)

residue (Fig. 2a and Supplementary Fig. S3). DNA binding was assessed by gel electrophoresis using pDNA containing a GFP expression construct to determine the amount of free DNA at different SWNT-PM-Peptide concentrations (Figs. 2 and Supplementary Fig. S3). For the SWNT-PM experiments, both SWNT-CytAib and SWNT-CytAibKH9 were successfully synthesized based on their observed DNA-binding curves, and the addition of Aib did not significantly affect the binding ability of the peptides either individually or after conjugation to the SWNTs (Fig. 2b and Supplementary Figs. S4, 5) compared with previous studies using only Cytcox [4]. We then evaluated the conjugation of CytAib to SWNT-PM by AFM and observed similar strand-like structures to those of previously observed SWNT-PM nanocarriers (Fig. 2c). Naked SWNTs had an average diameter of 0.81 ± 0.22 nm, which increased to 2.02 ± 0.6 nm upon polymer coating. Moreover, functionalization with Cytcox and KH9 peptides did not significantly change the overall height observed (2.14 ± 0.72 nm). Substitution of the Cytcox peptide with CytAib slightly increased the observed height to 2.60 ± 0.82 nm, but the difference was not statistically significant (Fig. 2c). Conjugation with either CytKH9 or CytAibKH9 resulted in similar physical characteristics, including similar secondary structures and AFM heights (Supplementary Fig. S6), suggesting that the overall SWNT-PM structure was not perturbed by Aib substitution within the Cytcox peptide and likely suggesting that the peptide secondary structure was maintained even upon functionalization, which is consistent with previous research showing that the peptide secondary structure could be maintained even after binding to nanoparticles, including gold and CNTs, which could mediate cellular entry [15, 34–36].

Improved permeability of SWNT-PM-CytAib

Next, we investigated the effect of CytAib on the permeability of SWNT-PMs. To quantify uptake within plants, we used a model plant cell, tobacco bright yellow (BY-2) cells,

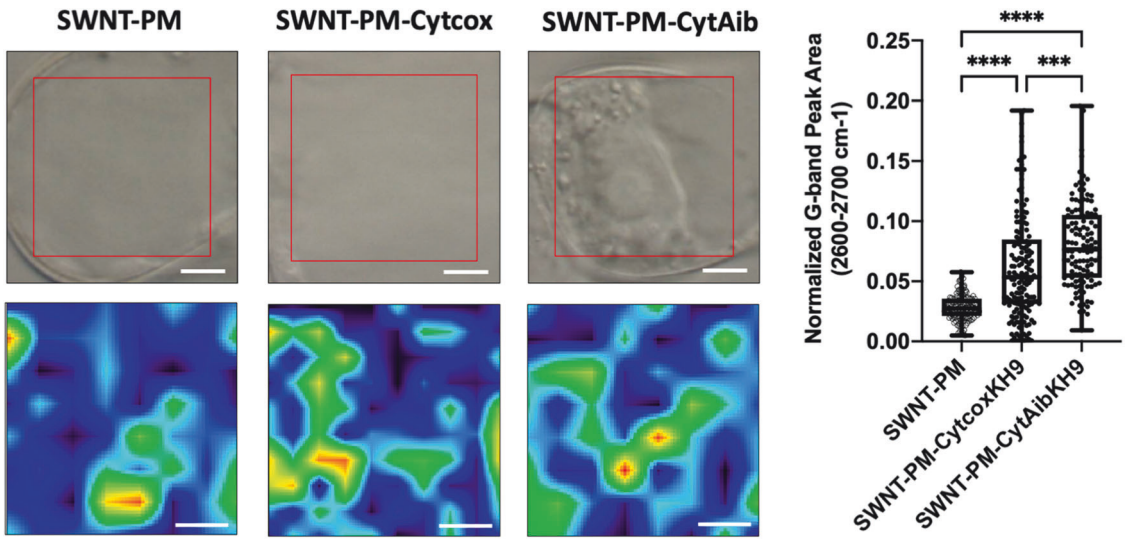

Fig. 3 Increased permeability of SWNT-PM-CytAib. Raman microscopy mapping of the G-band peaks of the SWNTs showing the uptake of SWNT-PM, SWNT-PM-Cytcox, and SWNT-PM-CytAib by BY-2 cells after 2 h of incubation. Normalized G-band peak areas were used to quantify their respective uptake levels and were obtained from five separate samples with a minimum of 20 spectra for each condition ($n = 5$). The statistical significance of differences between individual samples was determined by one-way ANOVA. The P values were <0.0001 and <0.001 for comparisons between SWNT-PM- and both SWNT-PM-Peptide-treated samples and between SWNT-PM-CytcoxKH9-treated and SWNT-PM-CytAibKH9-treated samples, respectively. ***$P < 0.001$, ****$P < 0.0001$. Scale bars represent 5 µm

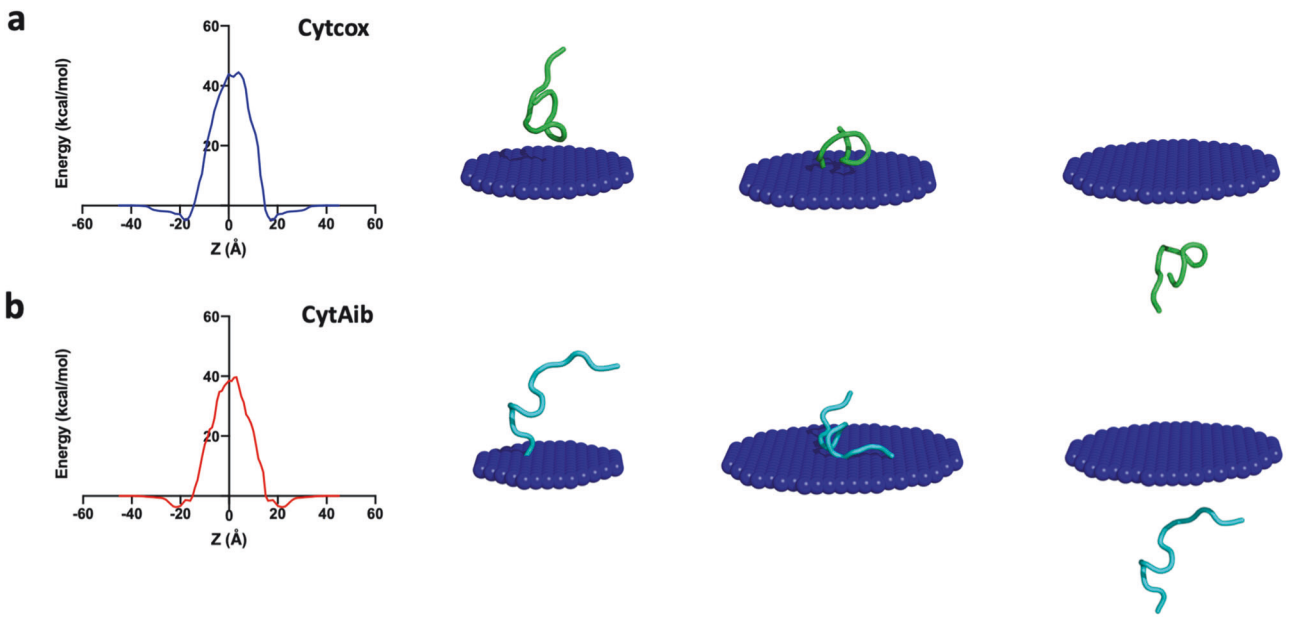

Fig. 4 Molecular modeling simulations of Cytcox and CytAib passing through model DOPC membranes. Molecular modeling simulations of (**a**) Cytcox and (**b**) CytAib peptides passing through a DOPC membrane and the corresponding calculated energies required for the respective passage through the membranes

for comparison among the different SWNT NCs. We incubated BY-2 cells with the respective SWNT NCs and quantified SWNT uptake through Raman microscopy (Fig. 3) [37, 38].

Due to the strong inherent Raman scattering of the SWNTs, which could be detected intracellularly, we quantified the intracellular uptake through the normalized G-band peak area at 2640 cm^{-1}, which corresponds to the SWNTs, as previously demonstrated [4]. Mapping of the three different samples revealed that both the SWNT-PM and SWNT-PM-Peptide samples could be taken up by BY-2 cells (Fig. 3). Samples incubated with SWNT-PM-Cytcox and SWNT-PM-CytAib showed significantly greater G-band signals than unfunctionalized SWNT-PM, with

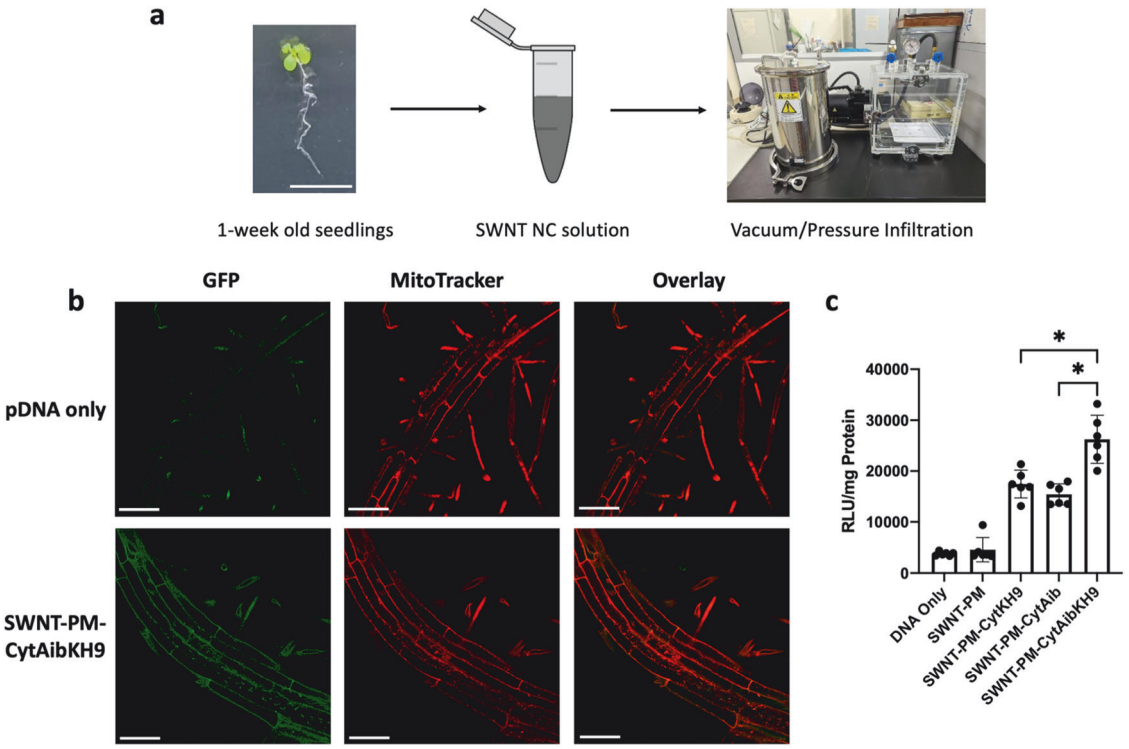

Fig. 5 GFP and luciferase reporter construct expression in *A. thaliana* infiltrated with SWNT-PM-Peptide NCs. a Schematic diagram showing the infiltration of SWNT NCs into 1-week-old *A. thaliana* seedlings using a vacuum/pressure infiltration setup. **b** Confocal microscopy images of *A. thaliana* 18 h post infiltration with SWNT-PM-CytAibKH9 showing mitochondrion-localized expression that colocalized with the MitoTracker label. Minimal fluorescence was observed for samples infiltrated with pDNA only. **c** Expression was quantified using a transient *Renilla* luciferase reporter construct delivered with different SWNT-PM-Peptide NCs. Whole seedling lysates were used to evaluate overall expression, and expression was observed in both SWNT-PMs functionalized with CytKH9 and those functionalized with CytAibKH9. The *P* values were 0.0342 for SWNT-PM-CytKH9 and SWNT-PM-CytAibKH9 and 0.0107 for SWNT-PM-CytAib and SWNT-PM-CytKH9. The data points from six biological replicates ($n = 6$) are presented as the means ± standard deviations. Statistical significance between individual samples was determined by one-way ANOVA with the Kruskal–Wallis test for multiple comparisons; $^*P < 0.05$. Scale bars represent 20 µm

G-band signals that were roughly three times greater than those observed for the nonfunctionalized samples. The average G-band area of the SWNT-PM-CytAibKH9 samples was approximately 10% greater than that of the SWNT-PM-CytKH9 samples, suggesting that the Aib substitution was able to confer greater cell-penetrating abilities to the peptide even after functionalization on the surface of the SWNTs.

We hypothesized that the increased uptake in the BY-2 cells may have been because the incorporation of Aib into the Cytcox peptide increased membrane permeability. We investigated this possibility through molecular modeling of the passage of the two peptides through model membranes (Fig. 4 and Supplementary Fig. S7). Modeling of their initial membrane interactions revealed that the helical structure induced by the Aib residues was able to mediate the initial interaction between the peptide and the membrane (Fig. 4b and Supplementary Movie 1). This interaction may have played a role in reducing the total energy required for the passage of the two peptides (Supplementary Fig. S7) and facilitating the interaction between the peptide and the membrane, as we showed that the overall peptide secondary structures were maintained even after functionalization on the SWNT surface; this effect is likely magnified when multiple peptides are conjugated to the surface of the SWNT, leading to increases in cell permeability and observed delivery efficiencies, as demonstrated in other nanoparticle studies [15, 39, 40].

pDNA delivery and expression by SWNT-PM-CytAib

Finally, we wanted to determine whether the improved membrane permeability led to a significant increase in gene delivery through the expression of two reporter constructs. First, we evaluated the delivery and specificity of the observed gene using a standard GFP reporter construct containing the mitochondrial promoter pATMTTF1. Delivery into intact 1-week-old *A. thaliana* was performed using standard vacuum/pressure infiltration (Fig. 5a). GFP was observed to colocalize efficiently with MitoTracker-labeled mitochondria (Fig. 5b). Compared with *A. thaliana* seedlings infiltrated with only pDNA or unconjugated CytAib/pDNA containing a GFP reporter

construct (Supplementary Fig. S8), SWNT-PM-CytAibKH9 seedlings showed mitochondria-localized GFP expression, suggesting that the pDNA was successfully delivered into the mitochondria and that the pDNA was released for expression. Next, to further quantify the expression levels of the SWNT NCs and evaluate the effects of Aib substitution on the Cytcox peptide, we evaluated the expression of the *Renilla luciferase* (RLuc) reporter construct (Fig. 5c). All three SWNT-PM-Peptide NCs were able to deliver the reporter construct pDNA for expression. Both the SWNT-PM-CytKH9 and SWNT-PM-CytAib samples had RLuc activity levels of approximately 15,000–17,000 ± 2000 RLU/mg protein. The addition of KH9 significantly increased the RLuc activity to 26,200 ± 4700 RLU/mg protein, possibly due to the additional pDNA binding capacity observed, which led to increased pDNA delivery. When comparing RLuc levels, we observed a significant increase in gene expression using SWNT-PM-CytAibKH9 (26,200 ± 4700 RLU/mg protein) compared with that of SWNT-PM-CytKH9 (17,400 ± 2700 RLU/mg protein), showing that the greater membrane permeability observed earlier for the CytAib peptide led to greater pDNA gene delivery and expression. Combined with the molecular dynamics and simulation results, this research suggests that the increased helical conformation induced by Aib can be used to increase the delivery efficiencies of known cell-penetrating or organelle-targeting peptide sequences.

Conclusion

In summary, we have successfully demonstrated that the substitution of Aib on Cytcox increased its cellular permeability, likely resulting in an increase in helical properties that facilitated the interaction of Cytcox with cellular membranes. The increase in permeability was maintained even upon conjugation to the SWNT-PM. The physical properties of CytAib, including its secondary structure and DNA binding properties, were similar to those of the original Cytcox peptide. Based on molecular dynamic simulations and Raman microscopy, Aib incorporation significantly increased the overall helical structure of the Cytcox peptide, suggesting that similar substitutions could be used to increase the cell permeability and delivery efficiencies of other nanocarriers where the overall secondary structures of functionalized peptides can be maintained.

Acknowledgements This work was funded by the Japan Science and Technology Agency Exploratory Research for Advanced Technology (JST-ERATO; Grant No. JPMJER1602), JST COI-NEXT (Grant No. JPMJPF2114), JSPS KAKENHI Grant-in-Aid for Transformative Research Areas A (A33002) and the MEXT Program: Data Creation and Utilization-Type Material Research and Development Project (Grant No. JPMXP1122714694).

Compliance with ethical standards

Conflict of interest The authors declare no competing interests.

Publisher's note Springer Nature remains neutral with regard to jurisdictional claims in published maps and institutional affiliations.

References

1. Ouyang B, Gu X, Holford P. Plant genetic engineering and biotechnology: a sustainable solution for future food security and industry. Plant Growth Regul. 2017;83:171–3.
2. Lv Z, Jiang R, Chen J, Chen W. Nanoparticle-mediated gene transformation strategies for plant genetic engineering. Plant J. 2020;104:880–91.
3. Yan Y, Zhu X, Yu Y, Li C, Zhang Z, Wang F. Nanotechnology Strategies for Plant Genetic Engineering. Adv Mater. 2022;34:2106945.
4. Law SSY, Liou G, Nagai Y, Giménez-Dejoz J, Tateishi A, Tsuchiya K et al. Polymer-coated carbon nanotube hybrids with functional peptides for gene delivery into plant mitochondria. Nat Commun. 2022;13:2417.
5. Demirer GS, Zhang H, Goh NS, González-Grandío E, Landry MP. Carbon nanotube–mediated DNA delivery without transgene integration in intact plants. Nat Protoc. 2019;14:2954–71.
6. Demirer GS, Zhang H, Matos JL, Goh NS, Cunningham FJ, Sung Y et al. High aspect ratio nanomaterials enable delivery of functional genetic material without DNA integration in mature plants. Nat Nanotechnol. 2019;14:456–64.
7. Wong MH, Misra RP, Giraldo JP, Kwak SY, Son Y, Landry MP et al. Lipid Exchange Envelope Penetration (LEEP) of Nanoparticles for Plant Engineering: A Universal Localization Mechanism. Nano Lett. 2016;16:1161–72.
8. Santana I, Jeon S-J, Kim H-I, Islam MR, Castillo C, Garcia GFH et al. Targeted Carbon Nanostructures for Chemical and Gene Delivery to Plant Chloroplasts. ACS Nano. 2022;16:12156–73.
9. Ficociello G, Salemme A, Uccelletti D, Fiorito S, Togna AR, Vallan L et al. Evaluation of the efficacy of carbon nanotubes for delivering peptides into mitochondria. RSC Adv. 2016;6:67232–41.
10. Zhang H, Goh NS, Wang JW, Pinals RL, González-Grandío E, Demirer GS et al. Nanoparticle cellular internalization is not required for RNA delivery to mature plant leaves. Nat Nanotechnol. 2022;17:197–205.
11. Law SSY, Miyamoto T, Numata K. Organelle-targeted gene delivery in plants by nanomaterials. Chem Commun 2023;59:7166–81.
12. Miyamoto T, Numata K. Advancing Biomolecule Delivery in Plants: Harnessing Synthetic Nanocarriers to Overcome

Multiscale Barriers for Cutting-Edge Plant Bioengineering. Bull Chem Soc Jpn. 2023;96:1026–44.
13. Squire HJ, Tomatz S, Voke E, González-Grandío E, Landry M. The emerging role of nanotechnology in plant genetic engineering. Nat Rev Bioeng. 2023;1:314–28.
14. Yoshizumi T, Oikawa K, Chuah JA, Kodama Y, Numata K. Selective Gene Delivery for Integrating Exogenous DNA into Plastid and Mitochondrial Genomes Using Peptide-DNA Complexes. Biomacromolecules. 2018;19:1582–91.
15. Wilder LM, Fies WA, Rabin C, Webb LJ, Crooks RM. Conjugation of an α-Helical Peptide to the Surface of Gold Nanoparticles. Langmuir. 2019;35:3363–71.
16. Miyamoto T, Tsuchiya K, Numata K. Endosome-escaping micelle complexes dually equipped with cell-penetrating and endosome-disrupting peptides for efficient DNA delivery into intact plants. Nanoscale. 2021;13:5679–92.
17. Misawa T, Ohoka N, Oba M, Yamashita H, Tanaka M, Naito M et al. Development of 2-aminoisobutyric acid (Aib)-rich cell-penetrating foldamers for efficient siRNA delivery. Chem Commun 2019;55:7792–5.
18. Gimenez-Dejoz J, Numata K. Molecular dynamics study of the internalization of cell-penetrating peptides containing unnatural amino acids across membranes. Nanoscale Adv. 2022;4:397–407.
19. Terada K, Gimenez-Dejoz J, Kurita T, Oikawa K, Uji H, Tsuchiya K et al. Synthetic Mitochondria-Targeting Peptides Incorporating α-Aminoisobutyric Acid with a Stable Amphiphilic Helix Conformation in Plant Cells. ACS Biomater Sci Eng 2021;7:1475–84.
20. Chuah J-A, Matsugami A, Hayashi F, Numata K. Self-Assembled Peptide-Based System for Mitochondrial-Targeted Gene Delivery: Functional and Structural Insights. Biomacromolecules. 2016;17:3547–57.
21. Chuah J-A, Yoshizumi T, Kodama Y, Numata K. Gene introduction into the mitochondria of Arabidopsis thaliana via peptide-based carriers. Sci Rep. 2015;5:7751.
22. von Heijne G. Mitochondrial targeting sequences may form amphiphilic helices. EMBO J. 1986;5:1335–42.
23. Dimogkioka A-R, Lees J, Lacko E, Tokatlidis K. Protein import in mitochondria biogenesis: guided by targeting signals and sustained by dedicated chaperones. RSC Adv. 2021;11:32476–93.
24. Kai M, Takeda K, Morita T, Kimura S. Distance dependence of long-range electron transfer through helical peptides. J Pept Sci. 2008;14:192–202.
25. Otoda K, Kitagawa Y, Kimura S, Imanishi Y. Chain length dependent transition of 310- to α-helix of Boc-(Ala-Aib)n-OMe. Biopolymers. 1993;33:1337–45.
26. Nagai Y, Tsutsumi Y, Nakashima N, Fujigaya T. Synthesis of Single-Walled Carbon Nanotubes Coated with Thiol-Reactive Gel via Emulsion Polymerization. J Am Chem Soc. 2018;140:8544–50.
27. Tsutsumi Y, Fujigaya T, Nakashima N. Polymer synthesis inside a nanospace of a surfactant–micelle on carbon nanotubes: creation of highly-stable individual nanotubes/ultrathin cross-linked polymer hybrids. RSC Adv. 2014;4:6318.
28. Singh S, Singh H, Tuknait A, Chaudhary K, Singh B, Kumaran S et al. PEPstrMOD: structure prediction of peptides containing natural, non-natural and modified residues. Biol Direct. 2015;10:73.
29. Lomize AL, Pogozheva ID, Mosberg HI. Anisotropic solvent model of the lipid bilayer. 2. Energetics of insertion of small molecules, peptides, and proteins in membranes. J Chem Inf Model. 2011;51:930–46.
30. Oeller M, Kang RJD, Bolt HL, Gomes dos Santos AL, Weinmann AL, Nikitidis A et al. Sequence-based prediction of the intrinsic solubility of peptides containing non-natural amino acids. Nat Commun. 2023;14:7475.
31. Longo E, Crisma M, Formaggio F, Toniolo C, Moretto A. Hydrophobic Aib/Ala peptides solubilize in water through formation of supramolecular assemblies. Polym J. 2013;45:516–22.
32. Tsuji G, Misawa T, Doi M, Demizu Y. Extent of Helical Induction Caused by Introducing α-Aminoisobutyric Acid into an Oligovaline Sequence. ACS Omega. 2018;3:6395–9.
33. Doig AJ. Chapter 1 - Stability and Design of α-Helical Peptides. Prog Mol Biol Transl Sci. 2008;83:1–52.
34. Heller DA, Pratt GW, Zhang J, Nair N, Hansborough AJ, Boghossian AA et al. Peptide secondary structure modulates single-walled carbon nanotube fluorescence as a chaperone sensor for nitroaromatics. Proc Natl Acad Sci. 2011;108:8544–9.
35. Brancolini G, Bellucci L, Maschio MC, Di Felice R, Corni S. The interaction of peptides and proteins with nanostructures surfaces: a challenge for nanoscience. Curr Opin Colloid Interface Sci. 2019;41:86–94.
36. Egorova EA, van Rijt MMJ, Sommerdijk N, Gooris GS, Bouwstra JA, Boyle AL et al. One Peptide for Them All: Gold Nanoparticles of Different Sizes Are Stabilized by a Common Peptide Amphiphile. ACS Nano. 2020;14:5874–86.
37. Liu Z, Zhang J, Gao B. Raman spectroscopy of strained single-walled carbon nanotubes. Chem Commun. 2009;6902–18, https://doi.org/10.1039/B914588E.
38. Dresselhaus MS, Dresselhaus G, Saito R, Jorio A. Raman spectroscopy of carbon nanotubes. Phys Rep. 2005;409:47–99.
39. Franco-Ulloa S, Guarnieri D, Riccardi L, Pompa PP, De Vivo M. Association Mechanism of Peptide-Coated Metal Nanoparticles with Model Membranes: A Coarse-Grained Study. J Chem Theory Comput. 2021;17:4512–23.
40. Leal J, Peng X, Liu X, Arasappan D, Wylie DC, Schwartz SH et al. Peptides as surface coatings of nanoparticles that penetrate human cystic fibrosis sputum and uniformly distribute in vivo following pulmonary delivery. J Control Rel. 2020;322:457–69.